SCIENTIFIC REPORTS

OPEN

Lanthanum hexaboride for solar energy applications

Elisa Sani[1], Luca Mercatelli[1], Marco Meucci[1], Luca Zoli[2] & Diletta Sciti[2]

Received: 30 November 2016
Accepted: 14 February 2017
Published online: 06 April 2017

We investigate the optical properties of LaB_6 – based materials, as possible candidates for solid absorbers in Concentrating Solar Power (CSP) systems. Bulk LaB_6 materials were thermally consolidated by hot pressing starting from commercial powders. To assess the solar absorbance and spectral selectivity properties, room-temperature hemispherical reflectance spectra were measured from the ultraviolet to the mid-infrared, considering different compositions, porosities and surface roughnesses. Thermal emittance at around 1100 K has been measured. Experimental results showed that LaB_6 can have a solar absorbance comparable to that of the most advanced solar absorber material in actual plants such as Silicon Carbide, with a higher spectral selectivity. Moreover, LaB_6 has also the appealing characteristics to be a thermionic material, so that it could act at the same time both as direct high-temperature solar absorber and as electron source, significantly reducing system complexity in future concentrating solar thermionic systems and bringing a real innovation in this field.

Lanthanum hexaboride (LaB_6) is a well known thermionic material (see for instance refs 1–5 among the many available). Its ability to emit electrons has been widely exploited in last 60 years since the pioneering work of Lafferty on sintered hexaboride ceramics[6]. It has been used to build hot cathodes for a large variety of applications, including electron guns in cathode tubes[7], cathodes for plasma production[8,9] and electron microscopes[10,11]. While at present, mainly single crystalline emitters are used, sintered ceramics show thermionic properties as well, and historically they have been the first to be studied[6,7,12]. It has been shown that, if surface impurities are removed, sintered LaB6 can show a work function value of 2.36 eV, which is fully comparable to that of single crystals (2.28 ÷ 2.47 eV)[13]. In addition, photo-induced electron emission is documented in the literature both by single crystals and by polycristalline specimens[14,15], as well as simultaneous thermionic emission and photoemission under excitation of a polycrystalline film at 442 nm wavelength (2.8 eV)[16].

In the field of material processing, LaB_6 is also used as additive to other diboride ultra-high temperature ceramics (UHTCs) for improving their oxidation resistance at extreme temperatures[17,18]. Because of its well-defined plasma reflection edge making it a textbook case, optical properties of bulk and thin film LaB_6 have been investigated and theoretically modeled in the past[19–21]. Recently, the attention on optical properties of LaB_6 has been renewed, but to the best of our knowledge, it is mainly restricted to the use of this material in form of nanoparticles[22–24].

Renewable energies, and in particular solar energy exploitation issues, are a key topic for the future. At present, the main technologies for concentrating solar systems are solar thermal power and concentrating photovoltaics. However, very recently a novel approach has been proposed for the direct generation of power from concentrated sunlight exploiting both thermionic and thermoelectric effects[25]. In the cited paper, the solar absorber and the thermionic emitter were different materials, with the thermionic emitter (a thin diamond film) deposed on the back surface of the sunlight absorber (an UHTC carbide with a special treatment to increase solar absorbance).

From our previous studies on UHTC carbides and borides[26–34], we have assessed strength and weakness points for the use of this class of novel materials as innovative high-temperature solar absorbers in thermodynamic solar plants. In fact, the ideal solar absorber should withstand very high temperatures while maintaining, with no damage, good mechanical strength and stability, high thermal conductivity, high solar absorbance to efficiently collect sunlight, and low emittance at operating temperatures, to minimize unwanted energy losses by thermal re-radiation[35–37]. From point of view of optical properties, strength points of UHTC materials we have investigated so far are the intrinsic low thermal emittance and good spectral selectivity, while solar absorbance typically is to be improved, e.g. by proper surface treatments[38,39]. In this work we report on the microstructural and optical

[1]CNR-INO National Institute of Optics, Largo E. Fermi, 6, I-50125, Firenze, Italy. [2]CNR-ISTEC, Institute of Science and Technology for Ceramics, Via Granarolo 64, I-48018, Faenza, Italy. Correspondence and requests for materials should be addressed to E.S. (email: elisa.sani@ino.it)

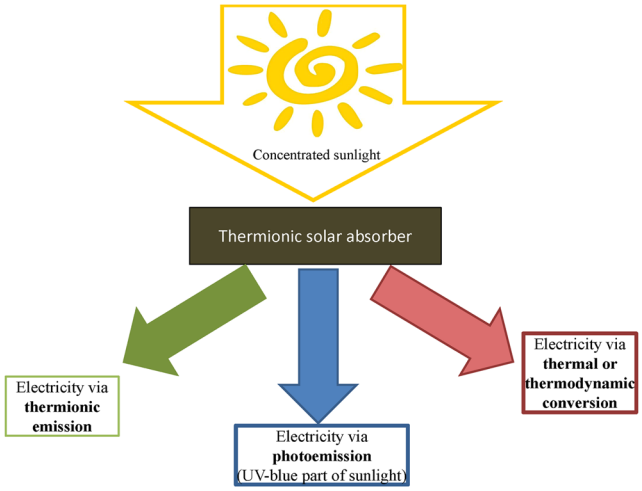

Figure 1. Concept of the thermionic/thermodynamic solar absorber.

Sample label	Composition Vol%	Description	Bulk density, relative density		Ra, Rt (μm)
			g/cm³	%	
LaB6_p rough	100% LaB_6	Porous, as sintered	3.7	80%	0.58 ± 0.06 4.70 ± 0.83
LaB6_p polished	100% LaB_6	Porous, Polished up to 1 μm	3.7	80%	0.09 ± 0.01 0.52 ± 0.09
LaB6_d polished	$LaB_6 + 15$ vol% $ZrB_2 + 3$ vol% B_4C	Dense, Polished up to 1 μm	4.86	100%	0.03 ± 0.01 0.19 ± 0.05

Table 1. List of materials, compositions, densities and surface roughness. The letter _p in the name stands for porous, while the suffix _d identifies the dense sample. R_a: mean surface roughness; R_t: distance between the highest asperity and the lowest valley.

characterization of LaB_6 ceramics. For thermodynamic solar applications, the knowledge of optical properties of LaB_6 is of interest because, as recalled above, it is used as additive for UHTC borides.

However, we point out that the innovation potential of LaB6 is much higher. In fact, compared to previously investigated UHTCs, LaB_6 has the appealing characteristics to be a thermionic material, so that it could act at the same time both as direct high-temperature solar absorber and as electron source, significantly reducing system complexity in future concentrating solar thermionic systems and bringing a real innovation in this field. Moreover, if surface impurities will be carefully controlled, e.g. with a proper control of production processes and with operation in vacuum, so that the work function is maintained below 4.13 eV (corresponding to light wavelengths longer than 300 nm), direct electron emission (photoemission) from LaB_6 induced by absorption of the UV-blue spectral portion of concentrated sunlight could be additionally and simultaneously exploited (Fig. 1). Thus, to assess the potential of LaB_6 for this radically new concept of solar absorber we carried out our study as a function of the sample porosity and surface finishing.

Results and Discussion

Microstructural features. Table 1 lists investigated samples, while Fig. 2 shows microstructures and EDS spectra. As expected, the monolithic material (LaB_6_p), Fig. 2a,b contains a significant fraction of open porosity, in agreement with density measurements. The grain size ranges from 3 to 10 μm. Traces of La-B-O spurious phases were recognized along the grain boundaries by SEM-EDS analysis. (see inset of Fig. 2b and corresponding EDS spectra). These impurities are typical contaminants of the boride powders and hindered the material densification during hot pressing[40].

From both Fig. 2a,b and Table 1 the difference of surface roughness between as sintered and polished surface can be appreciated (Ra decreased from 0.58 to 0.09 μm for unpolished and polished surfaces, respectively).

As for the LaB_6 _d sample, addition of ZrB_2 and B_4C notably improved the densification. The final material was completely dense and the microstructure can be observed in Fig. 2c–e. According to XRD (not shown) no extra phases formed. Dark spots in Fig. 2c,d belong to B_4C, while the in secondary electron imaging LaB_6 and ZrB_2 display similar contrast. By in-lens signal, see Fig. 2e, dark contrasting grains belong to LaB_6, whilst light contrasting grains belong to ZrB_2. The improvement in the densification was mainly attributed to the addition of B_4C, via cleaning of surface oxides such as La_xO_y, B_xO_y from the boride particles, as observed for similar ceramics[40]. Increase in the final density also affected the quality of surface polishing and consequently the final roughness decreased to Ra 0.03 μm, see Table 1.

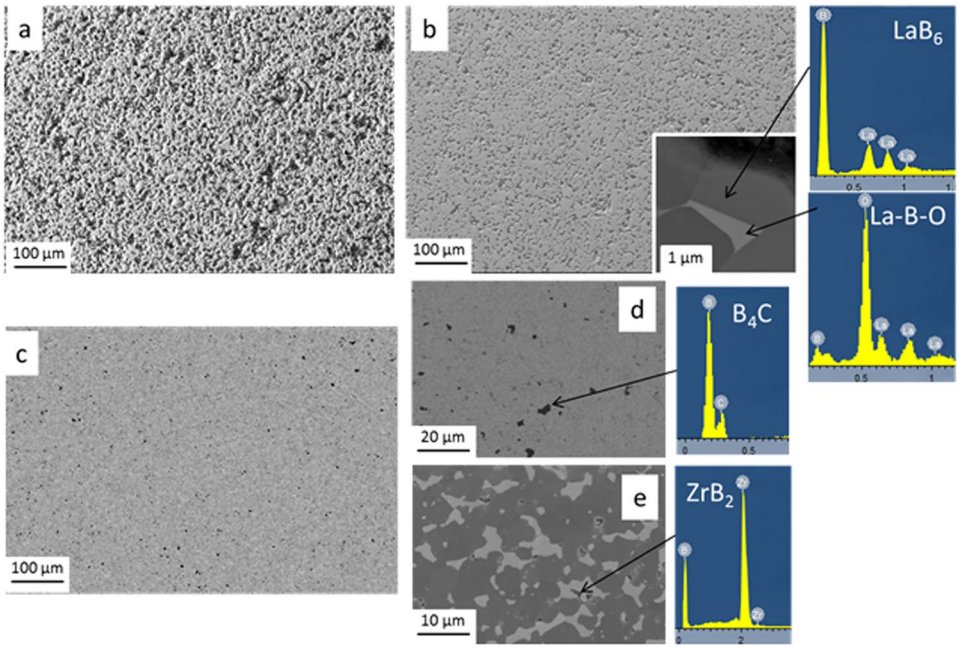

Figure 2. (**a**) Rough surface of porous LaB_6 in SE imaging, (**b**) polished surface of porous LaB_6 in SE imaging, Inset: high magnification of porous LaB_6 microstructure showing oxide phases (La_2O_3) wetting the grain boundaries and relative EDS spectra, (**c**) polished surface of dense LaB_6 in SE imaging, (**d**) higher magnification details showing B_4C pockets in BSE imaging; (**e**) ZrB_2 inclusion in LaB_6 matrix in-lens imaging (**d**) and corresponding EDS spectra.

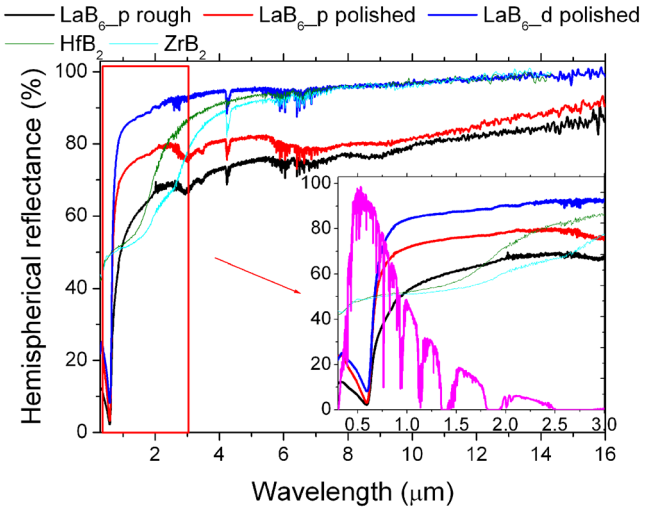

Figure 3. Reflectance spectra of samples, compared to dense samples of hafnium and zirconium borides from ref. 41.

Optical characterization. Figure 3 shows the reflectance spectra of LaB_6 samples, compared to previously analyzed dense hafnium and zirconium borides[41]. The inset of Fig. 3 shows the reflectance in the sunlight spectral region, the sunlight spectrum is also superimposed for reference.

LaB_6 reflectance directly increased with decreasing of the surface roughness. This is particularly evident comparing LaB_6_p rough and LaB_6_p polished. For the dense composite material, the reflectance was further improved due to the almost complete elimination of porosity. The spectrum shape presents very similar features in pure LaB_6 and the LaB_6 –based composite containing ZrB_2 and B_4C, except for a local minimum at round 3 µm wavelength and a couple of secondary small minima between 7 and 10 µm, present in both spectra of porous samples. These features could be ascribed to oxide phase impurities in porous LaB_6 ceramics, like La-O phases, B-O, or mixed La-B-O phases (as those observed in Fig. 2b). In contrast, these spurious phases were not observed in the optical spectra of LaB_6 _d owing to their removal by B_4C, as previously mentioned. No specific features in the spectrum that could be attributed to B_4C inclusions were recognized in LaB_6_d.

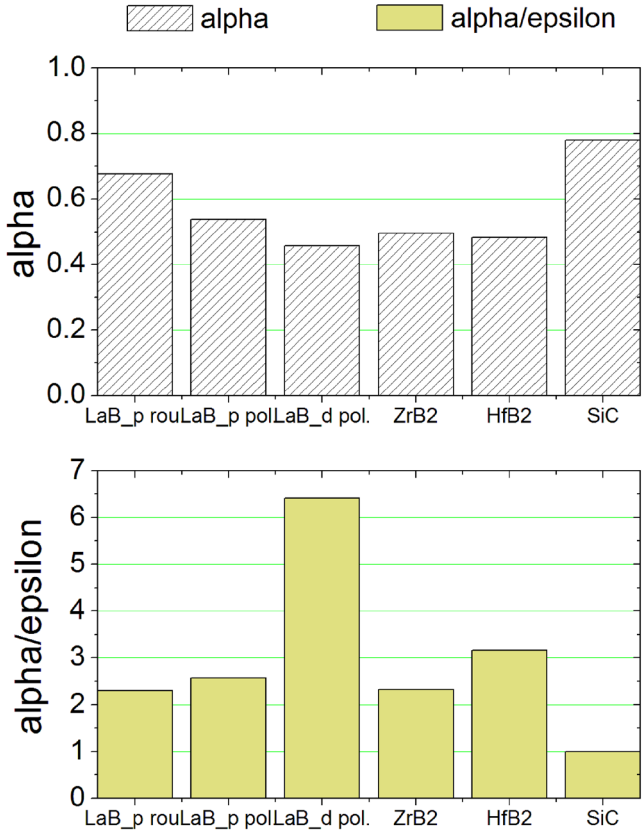

Figure 4. Calculated solar absorbance α and solar selectivity α/ε for LaB_6 samples and comparison with HfB_2, ZrB_2 and SiC.

Compared to hafnium and zirconium borides, LaB_6 has a considerable lower reflectance (i.e. a higher absorbance) near the peak of sunlight spectral distribution. However, thanks to peculiar spectral features of LaB_6, the rough porous sample, LaB_6_p rough remains more absorptive up to about 1 μm wavelength. Towards longer wavelengths, the reflectance of porous pellets is about 20% lower than that of other borides, while the dense sample shows a similar reflectance at the infrared plateau region.

From the experimental room-temperature hemispherical reflectance $\rho^{\cap}(\lambda)$ we calculated the total solar absorbance, α:

$$\alpha = \frac{\int_{\lambda_{min}}^{\lambda_{max}} (1 - \rho^{\cap}(\lambda)) \cdot S(\lambda) d\lambda}{\int_{\lambda_{min}}^{\lambda_{max}} S(\lambda) d\lambda} \quad (1)$$

where $S(\lambda)$ is the Sun emission spectrum[42] and the integration is carried out between $\lambda_{min} = 0.3\,\mu m$ and $\lambda_{max} = 3.0\,\mu m$; and an estimated hemispherical emittance, ε, at 1100 K:

$$\varepsilon = \frac{\int_{\lambda 1}^{\lambda 2} (1 - \rho^{\cap}(\lambda)) \cdot B(\lambda, 1100K) d\lambda}{\int_{\lambda 1}^{\lambda 2} B(\lambda, 1100K) d\lambda} \quad (2)$$

where $B(\lambda, 1100\,K)$ is the blackbody spectral radiance at 1100 K temperature and $\lambda 1 = 0.3\,\mu m$ and $\lambda 2 = 16.0\,\mu m$. The α/ε ratio (sometimes called spectral selectivity) is a parameter assessing the material potential for solar receiver applications, and ideally should be taken as high as possible. Figure 4 shows absorbance and spectral selectivity for the investigated LaB_6 samples, together with the two reference borides.

From Fig. 4 we can immediately appreciate the high potential of LaB_6 as solar absorber material: both solar absorbance and spectral selectivity are comparable or higher than those of comparison materials ZrB_2 and HfB_2[41]. Even more, the rough porous sample (LaB_6_p rough) shows a remarkable solar absorbance of 0.7, which is only slightly lower than that of the most advanced solar absorber material to date in actual plants, namely silicon carbide (SiC, $\alpha \approx 0.8$[41]) (see ref. 43 and references therein). As for spectral selectivity, for all samples it remains higher than that of SiC ($\alpha/\varepsilon \approx 1$[41]) and for most of them it is comparable to that of the two reference borides, with the LaB_6 dense polished sample showing a remarkable value of $\alpha/\varepsilon = 6.4$. If we compare LaB_6 pellets each other, we can say that a high solar absorbance is obtained at the expense of spectral selectivity. However, even in its less

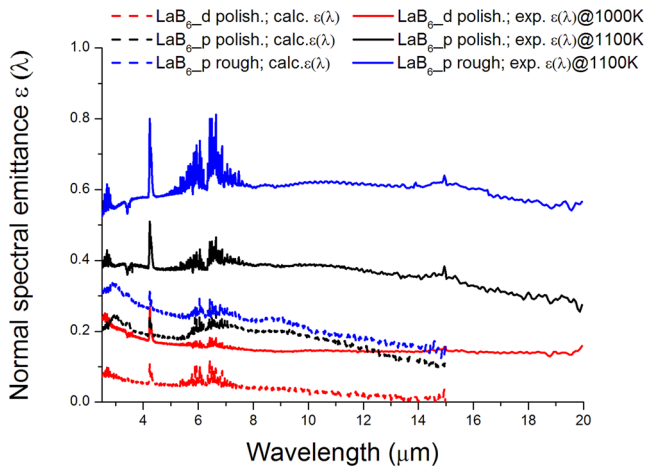

Figure 5. Calculated (dashed lines) and experimental emittance (solid lines) of LaB_6 samples. The measurement temperature for each sample is indicated in legend. The features at around 3.4 μm, 4.2 μm, between 4.8 and 7.7 μm and around 15 μm are instrumental artifacts due to unbalanced molecular absorption by ambient air in the optical path of the beams outside the furnace.

absorptive form (dense polished), LaB_6 results promising, as said before, with respect to previously investigated borides, as it shows a comparable absorbance and a remarkably higher spectral selectivity.

For a more reliable assessment of LaB_6 potential for solar absorber applications, we measured the thermal emittance at high temperature. In fact it is known that emittance calculated from room-temperature reflectance spectra are a very useful tool for a preliminary material evaluation, but underestimate the value at high temperature[44].

Figure 5 compares the experimental spectral normal emittances (solid lines) with the values calculated from room-temperature reflectance data $\varepsilon_{calc}(\lambda) = 1 - \rho^{\cap}(\lambda)$ (dashed values). As previously mentioned, the measured emittance is higher than the calculated one. Samples maintain the hierarchy among them, as expected, with the dense pellet showing the lowest emittance (spectrally integrated value of 0.2), the polished porous LaB_6 the intermediate value (0.4) and the rough porous the highest value (0.6). As a term of comparison, it should be noticed that LaB_6 favourably compares to SiC also if experimental emittances are considered, because the obtained values are significantly lower than those experimentally obtained for SiC pellets (0.9 at 1100 K).

If the spectral shape of emittance curves is concerned, we can observe that for the dense sample, calculated and experimental curves are very similar, while porous samples show some differences. In particular, for porous pellets, we cannot find in experimental emittances the wide bands of local maxima peaked at around 3, 7 and 9 μm wavelengths, that can be seen, on the contrary, in the curves calculated from room temperature spectra. Even if a quantitative evaluation requires additional microstructural measurements after high temperature experiments, which are beyond the scope of this work and will be the subject of a further study, we can explain the obtained results in terms of degassing of impurities still present in porous samples. For instance, according to studies carried out on the boron oxide vapor pressure[45], 1100 K and ~10^{-6} mbar cause boron oxide species vaporization in boride samples, which could be the case of the LaB6_p sample subjected to high vacuum/high temperature during the emissivity measurement.

In summary, the study we cave carried out both at room and high temperature show that LaB_6 not only is comparable or better than other boride UHTCs, but in its porous rough form is even better than SiC showing a similar solar absorbance and twice the spectral selectivity, as inferred from room temperature measurements, and a lower measured emittance at 1100 K temperature (0.6 versus 0.9). As already mentioned, SiC is the most advanced solar absorber actually used in plants to date.

Conclusions

This work is devoted to the study of the spectral reflectance and thermal emittance of pure LaB_6 and LaB_6-ZrB_2-SiC composites in order to evaluate their potential as novel solar absorbers. Pure LaB_6 materials contained a porosity of about 20%, which resulted in a lower reflectance compared to composite materials. In dense composites containing ZrB_2 as secondary phase, LaB_6 has an intrinsic solar radiation selectivity with high reflectance plateau at wavelengths longer than 1 μm and a remarkable α/ε ratio approaching 6.4. Moreover, the porous sample with rough surface favorably compares even to SiC from all points of view, as it shows a similar solar absorbance and a doubled spectral selectivity. Finally, if we consider the thermal emittance at 1000–1100 K temperature, even the most emissive LaB_6 porous rough sample has a significantly lower emittance than SiC.

However we emphasize that, in our opinion, the innovation potential of LaB_6 is much higher because, in addition to the promising characteristics listed above, it is also a widely documented thermionic material, and with one of the highest known electron emissivities. Thanks to these properties it could successfully act, at the same time, both as direct high-temperature solar absorber and as electron source, significantly reducing system complexity in future concentrating solar thermionic systems. This could make it a really revolutionary material in solar technology.

Methods

Commercial powders were used to produce the discs: LaB_6, (H.C. Starck Grade C), ZrB_2 (H.C. Starck, grade B), B_4C (H.C. Starck, grade HS). The monolithic LaB_6 was produced by hot pressing at 1930 °C, 40 MPa and holding time 15 min. The composite material was obtained by wet ball milling, drying of the starting powders with the following composition:

$$-LaB_6 + 15\ \text{vol\%}\ ZrB_2 + 3\ \text{vol\%}\ B_4C$$

The powder mixture was then densified by hot pressing at 1900 °C, 40 MPa and holding time 15 min. After sintering, the density of the ceramics was experimentally determined by the Archimede method. The sintered pellets were polished using diamond paste up to 1 μm. The samples' surface were analysed by SEM-EDS (FE-SEM, Carl Zeiss Sigma NTS Gmbh, Oberkochen, DE) and energy dispersive X-ray spectroscopy (EDS, INCA Energy 300, Oxford instruments, UK). The mean surface roughness (R_a) and the distance between the highest asperity, peak or summit, and the lowest valley (R_t) was measured according to the European standard CEN 624-4 using a commercial contact stylus instrument (Taylor Hobson mod. Talysurf Plus) fitted with a 2 μm-radius conical diamond tip over a track length of 8 mm and with a cut-off length of 0.8 mm.

The hemispherical reflectance spectra were acquired using two instruments: a double-beam spectrophotometer (Lambda900 by Perkin Elmer) equipped with a Spectralon®-coated integration sphere for the 0.25–2.5 μm wavelength region and a Fourier Transform spectrophotometer (FT-IR "Excalibur" by Bio-Rad) equipped with a gold-coated integrating sphere and a liquid nitrogen-cooled detector for the range 2.5–16.5 μm.

Thermal emittance has been measured using the setup described in detail in ref. 44 and here briefly recalled for convenience. The apparatus consists of a high-vacuum furnace interfaced either to a Fourier-transform infrared spectrophotometer (Bio-Rad Excalibur) and to a reference blackbody (C.I. Systems SR-2) by means of a splitting optical system. The ultimate pressure limit is few 10^{-6} mbar. The temperature is read on the sample upper surface by means of three thermocouples. The uncertainties are ±20 K on the temperature and ±5% on the spectral emittance. As for the temperature, it should be observed that the furnace heater is able to reach up to 1200 K, but the temperature obtained on the measurement surface of each sample is lower because of losses at thermal contact.

References

1. Oshima, C. *et al*. Thermionic emission from single-crystal LaB6 tips with [100],[110],[111], and [210] orientations. *Journal of Applied Physics* **51**, 1201–1206 (1980).
2. Futamoto, M. *et al*. Thermionic emission properties of a single-crystal LaB6 cathode. *Journal of Applied Physics* **51**, 3869–3876 (1980).
3. Storms, E. K. & Mueller, B. A. A study of surface stoichiometry and thermionic emission using LaB6. *Journal of Applied Physics* **50**, 3691–3698 (1979).
4. Futamoto, M., Nakazawa, M. & Kawabe, U. Thermionic emission properties of hexaborides. *Surface Science* **100**, 470–480 (1980).
5. Futamoto, M., Nakazawa, M. & Kawabe, U. High temperature surface composition of hexaboride thermionic electron emitters. *Vacuum* **33**, 727–732 (1983).
6. Lafferty, J. M. Boride Cathodes. *Journal of Applied Physics* **22**, 299–309 (1951).
7. Broers, A. N. Some experimental and estimated characteristics of the lanthanum hexaboride rod cathode electron gun. *Journal of Physics E: Scientific Instruments* **2**, 273 (1969).
8. Goebel, D. M., Crow, J. T. & Forrester, A. T. Lanthanum hexaboride hollow cathode for dense plasma production. *Review of Scientific Instruments* **49**, 469 (1978).
9. Akhmetov, T. D. *et al*. Studies of plasma production in a linear device with plane LaB_6 cathode and hollow anode. *AIP Conference Proceedings* **1771**, 070003 (2016).
10. Broers, A. N. High-resolution thermionic cathode scanning transmission electron microscope. *Applied Physics Letters* **22**, 610–612 (1973).
11. Zhang, H. *et al*. An ultrabright and monochromatic electron point source made of a LaB_6 nanowire. *Nature Nanotechnology* **11**, 273–279 (2016).
12. Furukawa, Y., Yamabe, M., Ishizuka, T. & Inagaki, T. Current stability of single-crystal and sintered LaB_6 cathodes. *Journal of Applied Physics* **52**, 533–534 (1981).
13. Pelletier, J. & Pomot, C. Work function of sintered lanthanum hexaboride. *Applied Physics Letters* **34**, 249–251 (1979).
14. Mogren, S. & Reifenberger, R. Thermionic and threshold photoemission energy distributions from LaB_6 (110). *Surface science* **186**, 232–246 (1987).
15. Zimmer, C. M. *et al*. Nanoscale photoelectron ionisation detector based on lanthanum hexaboride. *Physica status solidi (A)* **208**, 1241–1245 (2011).
16. May, P. G., Petkie, R. R., Harper, J. M. E. & Yee, D. S. Photoemission from thin-film lanthanum hexaboride. *Applied Physics Letters* **57**, 1584–1585 (1990).
17. Eakins, E., Jayaseelan, D. D. & Lee, W. E. Toward Oxidation-Resistant ZrB_2-SiC Ultra High Temperature Ceramics. *Metallurgical and Materials Transactions A* **42**, 878–887 (2011).
18. Zhang, X. H., Hu, P., Han, J. C., Xu, L. & Meng, S. H. The addition of lanthanum hexaboride to zirconium diboride for improved oxidation resistance. *Scripta Materialia* **57**, 1036–1039 (2007).
19. Kauer, E. Optical and electrical properties of LaB_6. *Physics Letters* **7**, 171 (1963).
20. Kimura, S., Nanba, T., Tomikawa, M., Kunii, S. & Kasuya, T. Electronic structure of rare-earth hexaborides. *Physical Reviews B* **46**, 12196–12204 (1992).
21. Peschmann, K. R., Calow, J. T. & Knauff, K. G. Diagnosis of the optical properties and structure of lanthanum hexaboride thin films. *Journal Applied Physics* **44**, 2252–2256 (1973).
22. Yuan, H. O. N. G. *et al*. Size dependent optical properties of LaB_6 nanoparticles enhanced by localized surface plasmon resonance. *Journal of Rare Earths* **31**, 1096–1101 (2013).
23. Yuan, Y., Zhang, L., Hu, L., Wang, W. & Min, G. Size effect of added LaB_6 particles on optical properties of LaB_6/polymer composites. *Journal of Solid State Chemistry* **184**, 3364–3367 (2011).
24. Chen, C. J. & Chen, D. H. Preparation of LaB_6 nanoparticles as a novel and effective near-infrared photothermal conversion material. *Chemical Engineering Journal* **180**, 337–342 (2012).
25. Bellucci, A. *et al*. Preliminary characterization of ST2G: Solar thermionic-thermoelectric generator for concentrating systems. *AIP Conference Proceedings* **1667**, 020007 (2015).

26. Sani, E., Mercatelli, L., Francini, F., Sans, J.-L. & Sciti, D. Ultra-refractory ceramics for high-temperature solar absorbers. *Scripta Materialia* **65**, 775–778 (2011).
27. Sani, E., Mercatelli, L., Fontani, D., Sans, J.-L. & Sciti, D. Hafnium and Tantalum Carbides for high temperature solar receivers. *Journal of Renewable and Sustainable Energy* **3**, 063107 (2011).
28. Sani, E., Mercatelli, L., Sansoni, P., Silvestroni, L. & Sciti, D. Spectrally selective ultra-high temperature ceramic absorbers for high-temperature solar plants. *Journal of Renewable and Sustainable Energy* **4**, 033104 (2012).
29. Sani, E., Mercatelli, L., Sans, J.-L., Silvestroni, L. & Sciti, D. Porous and dense Hafnium and Zirconium Ultra-High Temperature Ceramics for solar receivers. *Optical Materials* **36**, 163–168 (2013).
30. Sciti, D. *et al*. Tantalum diboride-based ceramics for bulk solar absorbers. *Solar Energy Materials and Solar Cells* **130**, 208–216 (2014).
31. Sani, E., Landi, E., Sciti, D. & Medri, V. Optical properties of ZrB_2 porous architectures. *Solar Energy Materials and Solar Cells* **144**, 608–615 (2016).
32. Sani, E. *et al*. Optical properties of dense zirconium and tantalum diborides for solar thermal absorbers. *Renewable Energy* **91**, 340–346 (2016).
33. Sani, E. *et al*. Compositional dependence of optical properties of zirconium, hafnium and tantalum carbides for solar absorber applications. *Solar Energy* **131**, 199–207 (2016).
34. Sani, E. *et al*. Process and composition dependence of optical properties of zirconium, hafnium and tantalum borides for solar receiver applications. *Solar Energy Materials and Solar Cells* **155**, 368–377 (2016).
35. Bogaerts, W. F. & Lampert, C. M. Materials for photothermal solar energy conversion. *Journal of Materials Science* **18**, 2847–75 (1983).
36. Lampert, C. M. Advanced optical materials for energy efficiency and solar conversion. *Sol. Wind Techn* **4**, 347–79 (1987).
37. Kennedy C. E. Review of mid- to high-temperature solar selective absorber materials. National Renewable Energy Laboratory report no. NREL/TP-520-31267 (2002).
38. Sciti, D. *et al*. Femtosecond laser treatments to tailor the optical properties of Hafnium carbide for solar applications. *Solar Energy Materials and Solar Cells* **132**, 460–466 (2015).
39. Sciti, D., Trucchi, D. M., Bellucci, A., Orlando, S., Zoli, L. & Sani, E. Effect of surface texturing by femtosecond laser on tantalum carbide ceramics for solar receiver applications. *Solar Energy Materials and Solar Cells* **161**, 1–6 (2017).
40. Sciti D., Silvestroni L., Medri V., Monteverde F. Sintering and densification of ultra-high temperature ceramics, In: Ultra-High Temperature Ceramics: Materials for Extreme Environment Applications, eds Fahrenholtz W., Wuchina E., Lee W., and Zhou Y., ISBN 0-471-9781118700785 Copyright © Wiley, Inc. 2014.
41. Sciti, D., Silvestroni, L., Mercatelli, L., Sans, J.-L. & Sani, E. Suitability of ultra-refractory diboride ceramics as absorbers for solar energy applications. *Solar Energy Materials and Solar Cells* **109**, 8–16 (2013).
42. Standard Tables for Reference Solar Spectral Irradiances: Direct Normal and Hemispherical on 37° Tilted Surface, Active Standard ASTM G173. ASTM G173 – 03 (2012).
43. Capuano, R. *et al*. Numerical models of advanced ceramic absorbers for volumetric solar receivers. *Renewable and Sustainable Energy Reviews* **58**, 656–665 (2016).
44. Mercatelli, L., Meucci, M. & Sani, E. Facility for assessing spectral normal emittance of solid materials at high temperature. *Applied Optics* **54**, 8700–8705 (2015).
45. Zhang, S. C., Hilmas, G. E. & Fahrenholtz, W. G. Pressureless densification of zirconium diboride with boron carbide additions. *J. Am. Ceram. Soc.* **89**, 1544–1550 (2006).

Acknowledgements

Part of this activity has been carried out in the framework of the FIRB2012-SUPERSOLAR project RBFR12TIT1 funded by the Italian Ministry of University and Research. E.S. gratefully acknowledges the Italian bank foundation "Fondazione Ente Cassa di Risparmio di Firenze" for supporting this activity within the framework of "SOLE NANO" project (pratica no. 2015.0861). Thanks are due to Mr. M. D'Uva, Mr. M. Pucci (CNR-INO) and C. Melandri (CNR-ISTEC) for technical assistance. Dr. N. Azzali (CNR-INO) is gratefully acknowledged for his help in thermal emittance measurements.

Author Contributions

D.S. and L.Z. prepared the samples and carried out microstructural analysis. E.S., L.M. and M.M. carried out optical characterization. E.S. and D.S. wrote the manuscript, which has been then reviewed by all authors.

Additional Information

Competing Interests: The authors declare that they have no competing interests.

Publisher's note: Springer Nature remains neutral with regard to jurisdictional claims in published maps and institutional affiliations.

Open Access This article is licensed under a Creative Commons Attribution 4.0 International License, which permits use, sharing, adaptation, distribution and reproduction in any medium or format, as long as you give appropriate credit to the original author(s) and the source, provide a link to the Creative Commons license, and indicate if changes were made. The images or other third party material in this article are included in the article's Creative Commons license, unless indicated otherwise in a credit line to the material. If material is not included in the article's Creative Commons license and your intended use is not permitted by statutory regulation or exceeds the permitted use, you will need to obtain permission directly from the copyright holder. To view a copy of this license, visit http://creativecommons.org/licenses/by/4.0/.

© The Author(s) 2017